3D Segmentation of Retinal Cysts from SD-OCT Images by the Use of three dimensional curvelet based K-SVD

Mahdad Esmaeili[1], Alireza Mehri Dehnavi [1], Hossein Rabbani [1], Fedra Hajizadeh [2]

[1] Isfahan University of Medical Sciences, Isfahan, Iran,[2] Noor Ophthalmology Research Center, Noor Eye Hospital, Tehran, Iran

mh_esmaeili@resident.mui.ac.ir, h_rabbani@med.mui.ac.ir, mehri@med.mui.ac.ir, fhajizadeh@noorvision.com

Abstract. This paper presents a new three dimensional curvelet transform based dictionary learning for automatic segmentation of intraretinal cysts, most relevant prognostic biomarker in neovascular age-related macular degeneration, from 3D SD-OCT images. In particular, we focus on the Spectralis SD-OCT (Heidelberg Engineering, Heidelberg, Germany) system, and show the applicability of our algorithm in segmentation of these features. For this purpose we use recursive gaussian filter and approximate the corrupted pixels from its surrounding, then in order to enhance the cystoid dark space regions and future noise suppression we introduce a new scheme in dictionary learning and take curvelet transform of filtered image then denoise and modify each noisy coefficients matrix in each scale with pre-defined initial 3D sparse dictionary. Dark pixels between RPE and NFL that were extracted with graph theory are considered as Cystoid spaces. The average dice coefficient for the segmentation of cystoid regions in whole 3D volume and within central 3 mm diameter in selected data set were found to be 0.65 and 0.77, respectively.

Keywords: Optical coherence tomography, Retinal Cysts, Speckle noise, Digital curvelet transform (DCUT), Dictionary learning.

1 Introduction

Spectral-domain optical coherence tomography (SD-OCT) is a rapidly developing noninvasive cross-sectional imaging modality which allows to investigate the presence of choroidal neovascularization(CNV) activity defined as the appearance of subretinal fluid, intraretinal cysts, intraretinal fluid, sub–retinal pigment epithelium fluid, or a combination thereof to assist the diagnosis and management of neovascular age-related macular degeneration (AMD)[1]. The intraretinal fluid spaces reduced retinal reflectivity than the surrounding tissues and can cause increased retinal thickness. Before segmentation of this regions in OCT images, the development of algorithmic approaches to provide noise suppression must be performed. In recent years, some approaches have been heavily investigated for speckle noise reduction, like aniso-

tropic diffusion-based methods [2-4], wavelet–based methods [5], dual tree complex wavelet transformation [6], curvelet transform [7], sparsity-based denoising [8,9]. Here, a novel speckle noise reduction algorithm is used[10], which is optimized to reduce speckle in an OCT image while maintaining strong edge sharpness. For this purpose we first apply recursive Gaussian filter to noisy image and zero possible pixels are approximated from surrounding pixels then we introduce K-SVD dictionary learning in curvelet transform domain for speckle noise reduction of 3D OCT images. As noise more affected low scale of curvelet coefficients and in order to take advantage of this sparse multiscale directional transform, we introduce a new scheme in dictionary learning and take curvelet transform of noisy image then denoise and modify each noisy coefficients matrix in each scale with pre-defined initial 3D sparse dictionary. The 3D initial dictionary for every scale in each rotation is independently selected from thresholded coefficients in the same scale and rotation of logarithmic transformation of image and doesn't need any high-SNR scans (averaged versions of repeated scans) for dictionary learning. After denoising 3D OCT images pixels in image are adjusted and thresholded to segment possible fluid space candidate pixels. Then nerve fiber layer (NFL) and retinal pigment epithelium (RPE) layer are extracted in each B-scan by the use of graph theory[11]. Identification of these lines is used to define our retinal regions of interest (ROI) in each B-mode image. Finally the possible false positives (FPs) are eliminated based on standard deviation and morphology of extracted candidate pixels.

The organization of this paper is as follows. Section 2 discusses the 3D curvelet based dictionary learning denoising algorithm, and section 3 shows an implementation of the algorithm for candidate cystoid space determination as well as our generalized method for removing miss extracted pixels, and results are presented in section 4. Finally, we conclude and give some perspectives for future work.

2 OCT Denoising

Although the direct analyzing of 3-D data as a volume and also considering the 3-D geometrical nature of the data is computationally expensive, but it has been shown that 3-D analysis of 3-D data outperforms 2-D slice-by-slice analyzing[12]. 3D curvelet elements are plate-like shapes of $2^{-j/2}$ in two directions and width about 2^{-j} in the orthonormal direction which are smooth within the plate and oscillates along the normal direction of the plate. The parabolic scaling, direction, tightness and sparse representation properties of this 3D multiscale transform, provide new opportunities to analyze large data sets in medical image processing. In this paper we used a new implementation of the 3D fast curvelet transform (3DFCT) [13,14] that has a reduced redundancy factor than the wrapping-based implementation as proposed in curvelab Toolbox [15,16] with the strong directional selectivity property at the finest scale.

For this purpose and taking curvelet coefficients:

1. Cartesian coronization is performed that decomposes the object into dyadic coronae based on concentric cubes. Each coronae is subdivided into trapezoidal regions conforming the usual parabolic scaling as shown in Fig.1.

2. The 3-D coefficients are obtained by applying an inverse 3D FFT to each wrapped wedge as shown in Fig.1, that appropriately fits into a 3-D rectangular parallelepipeds of dimensions ~ (2^j, $2^{j/2}$, $2^{j/2}$) centered at the origin.

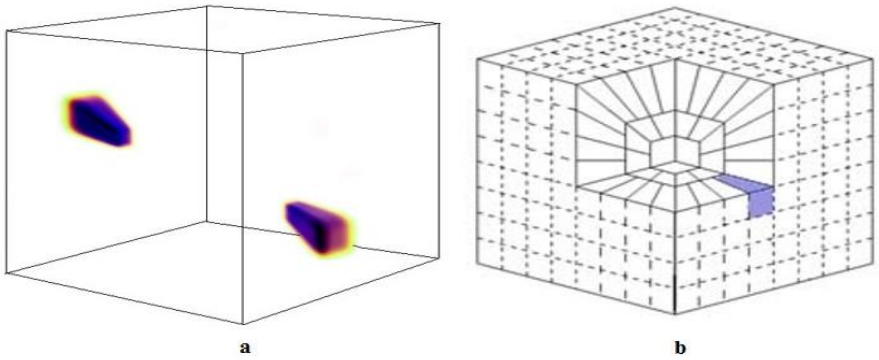

Fig. 1 3D rendering of Curvelet atom in frequency (a), and discrete frequency tiling (b), the shaded area separates 3D wedge.

Since the curvelet coefficients have a sparse distribution, we have only a few large coefficients that show the main structure of image and the remained coefficients tend to zero [15]. This transform maps signals and noise into different areas and signal's energy is concentrated in a limited number of coefficients in curvelet domain.

OCT denoising can improve the image quality for the accurate analysis of image information, such as intra-retinal layers and boundaries of pathology that the results of accurate detection of these features are fully dependent on image enhancement through image denoising [17,18]. For this purpose in our selected dataset all zero value corrupted pixels are determined from 5×5×5 surrounding pixels based on recursive Gaussian filter[19]. After removing zero pixels, we used a novel speckle noise reduction algorithm that was previously implemented on 3D, SD-OCT, Bioptigen imaging systems[10]. The our curvelet-based approach consists of first transforming the noisy image using the 3DFCT, and taking curvelet coefficients, then in curvelet domain for each scale and rotation the coefficient matrix is independently denoised based on K-SVD dictionary learning. A fundamental consideration in employing the KSVD dictionary learning is the selection of the start dictionary D. While some popular class of sparsity based denoising algorithms exploits the information of the noisy image itself to define the dictionary[8], however, the high-level of noise in the SDOCT images negatively contend with the learning process, degrades the quality of the trained dictionary. An alternative (ideal) approach is to learn the dictionary from the noiseless with high SNR image. Since in practice, such an ideal image is not available, so we select initial dictionary from thresholded curvelet coefficients in same scale and rotation of logarithmic transformation of noisy image (equation 1).

- The hard threshold T j,l is applied to each curvelet coefficients such that:

$$C(j,l,p) = \begin{cases} C(j,l,p) & if \quad C(j,l,p) \geq T_{j,l} \\ 0 & else \end{cases} \qquad (1)$$

The threshold Tj,l is selected based on so called k-sigma method [20], in which Tj,l=k×σ1×σ2, where k is an adjustable parameter, σ1 is the standard deviation of noise from a background region in the image data, and σ2 is the standard deviation of noise in the curvelet domain at a specific scale j and orientation l [20].

After finding the appropriate 3D initial dictionary, D, for each scale and orientation, the noisy curvelet coefficient matrixes of noisy image in same scale and rotation are despeckled based on K-SVD dictionary learning[11].

Since the curvelet transform is successful in dealing with edge discontinuities, it is a good candidate for edge enhancement. So, in order to enhance the contrast of intra-retinal layer boundaries, denoised curvelet coefficients, before taking 3D inverse discrete curvelet transform (3D-IDCUT), can be modified in order to enhance edges in an image [21,22]. A function must be defined which modifies the values of the curvelet coefficients by $k_C(C_{j,l,p})$ as follows:

$$k_C(x) = \begin{pmatrix} 2x & if \quad (x) < N \\ \left|\frac{x}{N}\right|^{0.3} x & if \quad N \le (x) < 3N \\ \left|\frac{M}{x}\right|^{0.5} x & if \quad 3N \le (x) \end{pmatrix} \qquad (2)$$

In this equation N=0.2M, here M is the maximum curvelet coefficient of the relative band. Then we reconstruct the enhanced image from the denoised and modified curvelet coefficients by applying IDCUT. The outline of the whole denoising process is shown in Fig. 2.

3 Candidate Cystoid Space Determination

In this section we present a new candidate detection algorithm to separate the dark spaces from the rest of the image. During this process, each pixel $f(i,j,k)$ in despeckled image is adjusted as follows:

$$g(i,j,k) = f(i,j,k) + .5\bar{f}_W - \frac{80(Max(f_W))}{Min(f_W)+1} \qquad (3)$$

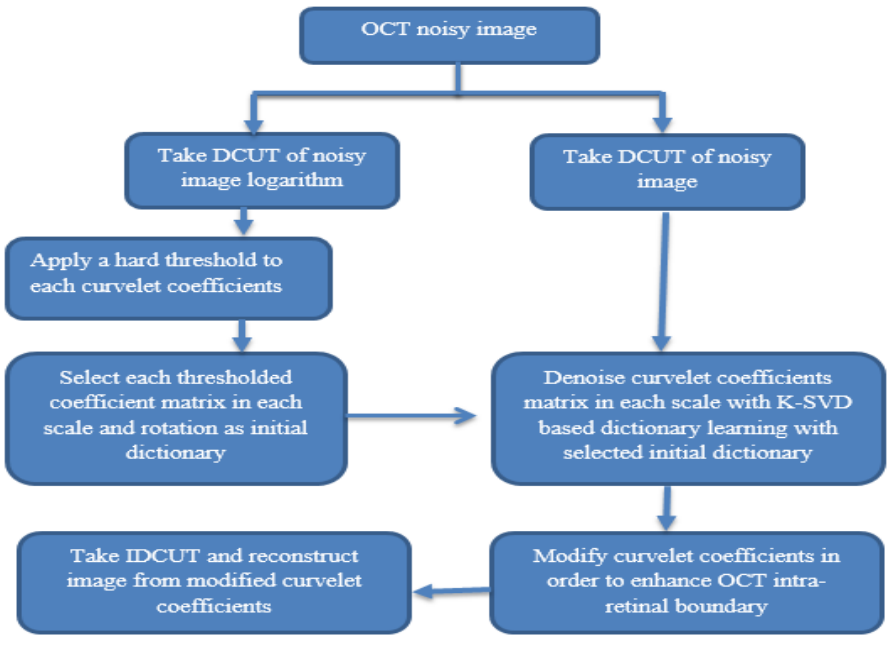

Fig. 2. The outline of the proposed method for despeckling

where $\bar{f}_W$, $Max(f_W)$ and $Min(f_W)$ are the mean, maximum and minimum intensity value of the image within a window W of size 3 × 3× 3 respectively. The dark cystoid spaces in adjusted image is trend to zero and extracted by applying simple threshold (t=5).

3.1 Removing Miss Extracted Pixels

In order to improve the specificity, we reject FP pixels by extracting nerve fiber layer (NFL) and retinal pigment epithelium (RPE) layer in each B-scan by the use of graph theory[23]. We use these extracted lines to define the upper and lower bounds as retinal region of interest (ROI) in which we segment the cystoid fluid. Then we define and calculate the F ratio[24] and remove every connected component in ROI that has F>4. This selection remove each connected component that has line shape structure belongs to dark regions between Outer Plexiform Layer (OPL) and Outer Nuclear Layer (ONL). Fig.3 depicts the evaluation of F.

$$F = \frac{\max(m_i, m_j)}{\min(M_i, M_j)} \tag{4}$$

where, $M_i = \max(\textit{width of a connected component in direction } i)$ and $M_j = \max(\textit{width of a connected component in direction } j)$ with $m_i = \max(i) - \min(i), \quad m_j = \max(j) - \min(j).$

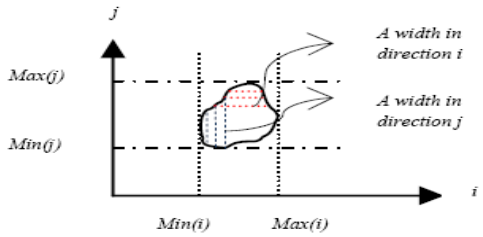

Fig. 3. Illustration of the evaluation F

The distribution of pixel intensity in cystoid spaces are also uniform[25] so final cystoid volumes are extracted by rejecting regions with a standard deviation greater than an empirically determined value of 30.

4 Experimental Results

This study has focused on OCT images obtained from spectralis SD-OCT (Heidelberg Engineering, Heidelberg, Germany) system. To evaluate the performance of this automated method, the method was applied on four 3D-OCT images each contain 49 B-scans, and the dice coefficients[26] of the segmented cystoid regions entire 3D volume,

were compared against the two manually labelled grader. Fig 4 show the results of our proposed algorithm.

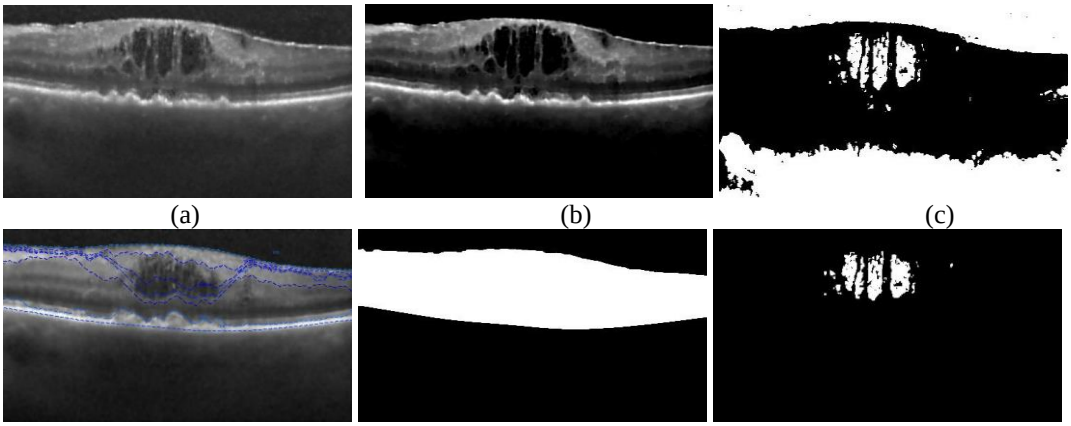

(a) (b) (c)

(d) (e) (f)

Fig.4. Results of our proposed method. (a) Despeckled image, (b) Adjusted image (c) Candidate cystoid pixels (d) Detected ILM and RPE and other layers with graph theory (e) Extracted ROI (f) Segmented cystoid pixels

Table 1. Evaluation of proposed method on against the two manually labelled grader.

Evaluation using		Grader 1	Grader 2	intersection of Graders 1 & 2
Dice coefficient(s)	spectralis_1	0.7140	0.6817	0.7181
	spectralis_2	0.4549	0.4581	0.4501
	spectralis_3	0.6954	0.6501	0.6846
	spectralis_4	0.7115	0.7255	0.7307
Dice coefficient within central 3 mm diameter	spectralis_1	0.8173	0.7792	0.7918
	spectralis_2	0.7775	0.7769	0.7493
	spectralis_3	0.7563	0.7823	0.7652
	spectralis_4	0.7528	0.7732	0.7710

5 Conclusion

This paper presented a new method for segmentation and quantify the total volume occupied by intraretinal cystoid fluid from 3D OCT image. We tested our algorithm on four 3D Spectralis SD-OCT (Heidelberg Engineering, Heidelberg, Germany) images, each contain 49 B-scans. In this paper we use the graph theory for extraction of of NFL and RPE, the upper and lower bounds as retinal region of interest, in order to increase the accuracy of detected bounds. In the presence of epiretinal membrane (ERM), a fine piece of scar tissue that grows on the surface of the retina, some FPs extracted that should be distinguish from intraretinal cysts. However the proposed method revealed promising results, but further validation studies with larger samples are needed.

References

1 Hee, M. R. *et al.* Quantitative assessment of macular edema with optical coherence tomography. *Archives of ophthalmology* **113**, 1019-1029 (1995).

2 Aja, S., Alberola, C. & Ruiz, J. Fuzzy anisotropic diffusion for speckle filtering. *IEEE International Conference on Acoustics, Speech, and Signal Processing,(ICASSP'01)* **2**, 1261-1264 (2001).

3 Puvanathasan, P. & Bizheva, K. Interval type-II fuzzy anisotropic diffusion algorithm for speckle noise reduction in optical coherence tomography images. *Optics express* **17**, 733-746 (2009).

4 Yu, Y. & Acton, S. T. Speckle reducing anisotropic diffusion. *Image Processing, IEEE Transactions on* **11**, 1260-1270 (2002).

5 Luisier, F., Blu, T. & Unser, M. A new SURE approach to image denoising: Interscale orthonormal wavelet thresholding. *Image Processing, IEEE Transactions on* **16**, 593-606 (2007).

6 Chitchian, S., Fiddy, M. A. & Fried, N. M. Denoising during optical coherence tomography of the prostate nerves via wavelet shrinkage using dual-tree complex wavelet transform. *Journal of Biomedical Optics* **14**, 014031-014031-014036 (2009).

7 Jian, Z. *et al.* Speckle attenuation in optical coherence tomography by curvelet shrinkage. *Optics letters* **34**, 1516-1518 (2009).

8 Elad, M. & Aharon, M. Image denoising via sparse and redundant representations over learned dictionaries. *Image Processing, IEEE Transactions on* **15**, 3736-3745 (2006).

9 Fang, L. *et al.* Sparsity based denoising of spectral domain optical coherence tomography images. *Biomedical optics express* **3**, 927-942 (2012).

10 M. Esmaeili, A. M. Dehnavi, H. Rabbani & Hajizadeh, F. 3D Curvelet Based Dictionary Learning for Speckle Noise Reduction of Optical Coherence Tomography. *submitted* (2015).

11 Aharon, M., Elad, M. & Bruckstein, A. The K-SVD: An Algorithm for Designing Overcomplete Dictionaries for Sparse Representation. *Signal Processing, IEEE Transactions on* **54**, 4311-4322 (2006).

12 Rabbani, H., Sonka, M. & Abramoff, M. D. Optical Coherence tomography noise reduction using anisotropic local bivariate Gaussian mixture prior in 3D complex wavelet domain. *Journal of Biomedical Imaging* **2013**, 22 (2013).

13 Woiselle, A., Starck, J.-L. & Fadili, J. 3-D Data Denoising and Inpainting with the Low-Redundancy Fast Curvelet Transform. *Journal of Mathematical Imaging and Vision* **39**, 121-139 (2011).

14 Woiselle, A., Starck, J.-L. & Fadili, J. 3D curvelet transforms and astronomical data restoration. *Applied and Computational Harmonic Analysis* **28**, 171-188 (2010).

15 Candes, E., Demanet, L., Donoho, D. & Ying, L. Fast discrete curvelet transforms. *Multiscale Modeling & Simulation* **5**, 861-899 (2006).

16 Ying, L., Demanet, L. & Candes, E. 3D discrete curvelet transform. *Applied and Computational Mathematics* **50** (2005).

17 Bonesi, M., Proskurin, S. & Meglinski, I. Imaging of subcutaneous blood vessels and flow velocity profiles by optical coherence tomography. *Laser Physics* **20**, 891-899 (2010).

18 Kajić, V. *et al*. Robust segmentation of intraretinal layers in the normal human fovea using a novel statistical model based on texture and shape analysis. *Optics express* **18**, 14730-14744 (2010).

19 Roomi, S. M. M., Lakshmi, I. & Kumar, V. A. A recursive Gaussian weighted filter for impulse noise removal. *GVIP Journal* **6**, 33-37 (2006).

20 Starck, J.-L., Candès, E. J. & Donoho, D. L. The curvelet transform for image denoising. *Image Processing, IEEE Transactions on* **11**, 670-684 (2002).

21 Esmaeili, M., Rabbani, H. & Dehnavi, A. M. Automatic optic disk boundary extraction by the use of curvelet transform and deformable variational level set model. *Pattern Recognition* **45**, 2832-2842 (2012).

22 Esmaeili, M., Rabbani, H., Mehri, A. & Dehghani, A. Extraction of retinal blood vessels by curvelet transform. *16th IEEE International Conference on Image Processing (ICIP),*, 3353-3356 (2009).

23 Chiu, S. J. *et al*. Automatic segmentation of seven retinal layers in SDOCT images congruent with expert manual segmentation. *Optics express* **18**, 19413-19428 (2010).

24 Esmaeili, M., Rabbani, H., Dehnavi, A. M. & Dehghani, A. in *Image Processing (ICIP), 2010 17th IEEE International Conference on*. 4093-4096 (IEEE).

25 Wilkins, G. R., Houghton, O. M. & Oldenburg, A. L. Automated segmentation of intraretinal cystoid fluid in optical coherence tomography. *Biomedical Engineering, IEEE Transactions on* **59**, 1109-1114 (2012).

26 Dice, L. R. Measures of the amount of ecologic association between species. *Ecology* **26**, 297-302 (1945).